The role of diazacrown ether in the enhancement of the biological activity of silver nanoparticles

Sarvinaz HAJIYEVA[1,*] ⓘ, **Ulviyya HASANOVA**[1] ⓘ, **Zarema GAKHRAMANOVA**[2] ⓘ,
Aygun ISRAYILOVA[3] ⓘ, **Khudaverdi GANBAROV**[3] ⓘ, **Eldar GASIMOV**[4] ⓘ, **Fuad RZAYEV**[4] ⓘ,
Goncha EYVAZOVA[5] ⓘ, **Alakbar HUSEYNZADA**[1] ⓘ, **Gunel ALIYEVA**[5] ⓘ, **Ilaha HASANOVA**[6] ⓘ,
Abel MAHARRAMOV[1] ⓘ

[1]Department of Organic Chemistry, Faculty of Chemistry, Baku State University, Baku, Azerbaijan
[2]Chemical Sensors and Reagents Laboratory, Azerbaijan State Oil and Industry University, Baku, Azerbaijan
[3]Department of Microbiology, Faculty of Biology, Baku State University, Baku, Azerbaijan
[4]Electron Microscopy Laboratory, Azerbaijan Medical University, Baku, Azerbaijan
[5]Nanoresearch Center, Baku State University, Baku, Azerbaijan
[6]Metal Complex Catalysts Laboratory, Faculty of Chemistry, Baku State University, Baku, Azerbaijan

Abstract: The nanostructuring of hydroxyl-substituted diazacrown-ether (DC) by silver nanoparticles was obtained by green synthesis method in order to increase the antibacterial activity of silver nanoparticles. The synthesized DC, nanoparticles, and nanosupramolecular complex (Ag@DC) were studied by TEM, powder-XRD, and NMR, IR, and UV spectroscopy methods. The Ag@DC nanostructures were uniform and their sizes ranged from 8 to 18 nm. IR and UV spectra revealed the noncovalent formation of the nanosupramolecular complex. The antibacterial activities of the prepared active agents were investigated on gram-positive and gram-negative bacteria by twofold microdilution method. Ultrastructural study by TEM was performed on *E. coli* BDU12 after treatment with Ag@DC. The results showed the improvement of the antibacterial action of Ag@DC compared to silver nanoparticles (*E. coli* BDU12 – 32 times, *A. baumannii* BDU32 – 16 times, *K. pneumoniae* BDU44 and *P. aeruginosa* BDU49 – 4 times, *S. aureus* BDU23 – 512 times). Chelating by DC significantly improved the antibacterial effects of the silver nanoparticles on gram-positive and gram-negative bacteria due to the ionophoric behavior of the crown ethers.

Key words: Silver nanoparticles, diazacrown ether, transmission electron microscopy, ultrastructural microscopy, antibacterial activity

1. Introduction

Silver nanoparticles have already found applications in different areas of study due to their unique features, such as optical, electrical, antibacterial, and thermal properties [1–4]. There are different methods for obtaining silver nanoparticles, based on chemical reduction, biochemical processes in plants and bacteria, and ecofriendly methods [5,6]. Their use as water-treatment agents and in membrane filtration processes also draws the scientific world's attention because of the wide-spectrum antimicrobial activity of silver nanoparticles, their cost-effectiveness, and the low chance of toxic byproduct formation in comparison with traditional chemical water-treatment agents [7–9]. Medical applications of zero-valent silver nanoparticles include biosensors, biological tags, disinfectants, and antibacterial coatings for various medical instruments, catheters, and devices [10–16].

---

*Correspondence: sarvinazhajiyeva@gmail.com

However, despite the wide-ranging benefits of using silver nanoparticles, there are also limitations in their medical applications [17]. There are still insufficient data on the safety of zero-valent silver nanoparticles for human use because the mechanisms of their action have not been thoroughly investigated. There are studies that show the toxicity of silver NPs not only on pathogenic cells but also on human cells, connected with the transition of Ag^0 ions to Ag^+. Some researchers supposed that this problem could be solved by applying different coating materials (surfactants) or chelators [18,19].

Diazacrown ethers, as representatives of supramolecular compounds, are also promising antibacterial active substances because of their ionophoric features. Crown ethers can act as chelating agents and influence the properties of nanoparticles by chelating them, therefore making it possible to minimize the toxic and adverse effects of silver nanoparticles [20,21].

Considering all of these points, it was interesting to perform the chelation of silver nanoparticles by diazacrown-ether (DC) and compare their biological activity with that of pure silver nanoparticles and pure diazacrown-ether (DC).

2. Materials and methods

2.1. Fourier transform infrared (FTIR) spectroscopy

FTIR spectra of Ag@DC NPs were recorded on a Varian 3600 FTIR spectrophotometer in KBr tablets. The spectra were taken in the range of 4000–400 cm^{-1} at room temperature.

2.2. Ultraviolet-visible (UV-Vis) spectroscopy

The UV-spectra were recorded on a Varian Cary 50 UV-Vis spectrophotometer. UV spectra were recorded in the range of 220–400 nm of both ethanol solutions of DC and Ag@DC nanostructures.

2.3. Powder X-ray diffraction (XRD) analysis

XRD study was performed on a Rigaku Mini Flex 600 XRD diffractometer under ambient conditions. CuKα radiation from a Cu X-ray tube (15 mA; 30 kV) was used. The samples were scanned in the Bragg angle 2 theta range of 30° to 80°.

2.4. Synthesis of 7,8,14,15,16,17,18,19-octahydro-6H-dibenzo[f,n][1,5,9,12] dioxadiazacyclopentadecin-7-ol (diazacrown ether or DC)

The synthesis of diazacrown was performed according to the procedure described by Hasanova et al. [20]. Yield of the product was 65%, mp 148–149 °C. Found: C 69.5, H 7.4, N 8.7%. Calculated for $C_{19}H_{24}N_2O_3$: C 69.5, H 7.4, N. 8.5%. IR (KBr): 3350 (OH); 3330, 1455 (NH); 1604, 1590, 1492 (Ar); 1255, 1035 (Ar-O-CH$_2$); 754 (1,2-Ar) cm^{-1}. ^{1}H NMR (d): 2.64 (s, 4H, NCH$_2$CH$_2$N), 3.24 (br, 3H, NH and OH), 3.65 (s, 4H, ArCH$_2$), 4.14 (m, 5H, CH$_2$CHCH$_2$), 6.74–7.25 (m, 8H, ArH) ppm.

2.5. 2.5. Synthesis of silver nanoparticles and nanosupramolecular ensemble Ag@DC

Ecofriendly and safe Ag^0 nanoparticles were obtained by a green synthesis method using starch [22]. To 30 mg of AgNO$_3$ was added 25 mg of starch, dissolved in 50 mL of distilled water. After that, 25% ammonia was added until the pH reached 11. The resulting solution was sonicated for 1 h with in an ice bath. Obtained

nanoparticles were dried at ambient temperature. From the powder was prepared a solution in distilled water, to which the diazacrown-ether was added at a ratio of 2:1 with further ultrasonication for 15 min. Samples were investigated by FTIR, XRD, and TEM and their antibacterial activities were compared.

2.6. Transmission electron microscopy (TEM)

The TEM analysis of compounds and biological samples was performed on a TEM JEOL-1400.

2.7. Antibacterial studies

The antimicrobial activity of the Ag@DC ensemble was tested against bacterial strains (*Acinetobacter baumannii* BDU32, *Escherichia coli* BDU12, *Klebsiella pneumoniae* BDU44, *Pseudomonas aeruginosa* BDU49, and *Staphylococcus aureus* BDU23) by the twofold microdilution method (96-well microtiter assay). The bacterial strains were taken from the culture collection of the Department of Microbiology (Baku State University, Azerbaijan). In this assay, we used U-bottomed 96-well microtiter plates. The inoculum was prepared from a fresh colony on Muller Hinton medium ("Liofilchem") and bacterial strains (1×10^5 CFU) were inoculated into each well of the microplate, which contained active agents at different concentrations ranging from 256 to 2 μg mL^{-1} for Ag and DC and 8 to 0.0625 μg mL^{-1} for Ag@DC. The Ag^0 nanoparticles and Ag@DC were dissolved in distilled water and sonicated for 15 min (20 kHz, ampacity power 87%, 500 W). The DC sample was dissolved in distilled water without further sonication. The growth was determined by the resazurin method after 24 h of incubation at 37 °C; 30 μL of resazurin solution (0.01%; Sigma Aldrich) was added to each well and the microplates were reincubated at 37 °C for about 4 h. If the color change from blue to pink, it indicated the growth of bacteria, and the minimum inhibitory concentration (MIC) was determined as the lowest concentration of the active agents that prevented this change in color [23,24].

2.8. Preparation of microbiological samples for TEM study

The influence of Ag^0 nanoparticles and the Ag@DC ensemble on the ultrastructural changes of *E. coli* BDU12 was investigated by TEM. *E. coli* BDU12 cells treated with 0.5 Ag@DC (0.5 μg mL^{-1} Ag : 0.25 μg mL^{-1} DC) and 0.25 Ag@DC (0.25 μg mL^{-1} Ag : 0.125 μg mL^{-1} DC) and untreated control *E. coli* BDU12 were incubated in a shaker (150 rpm) for 24 h at 37 °C. After that incubation, samples were centrifuged at 4500 rpm for 10 min. The resulting pellets were fixed in phosphate buffer solution (pH 7.4) containing 2% paraformaldehyde, 2% glutaraldehyde, and 0.1% picric acid. After postfixation procedures in 1% osmic acid solution for 1.5 h, Araldite-Epon blocks were prepared according to the generally accepted methods in electron microscopy [25]. Semithin sections (1–2 μm) were obtained with a Leica EM UC7 ultramicrotome for further investigation by light microscope (Primo Star, Zeiss) and photographed with a digital camera (Canon D650). Unstained ultrathin sections (50–60 nm) were examined under the JEM-1400 TEM at 80–120 kV. Morphometric analysis of the images (electronograms) was carried out in TIF format via a computer program (TEM Imaging Platform) developed by Olympus Soft Imaging Solutions GmbH (Germany).

3. Results

Synthesis of diazacrown ether was performed as shown in the Scheme. In the first stage of the synthesis, the condensation reaction of salicylaldehyde (**1**) was conducted with 1,2-ethylenediamine (**2**) in order to obtain the

product N, N-ethylenebis(salicylimine) (**3**). The reduction of **3** was followed by the ring closure reaction of **4** with 1,3-dichloro-2-propanol, resulting in formation of the final product (**5**).
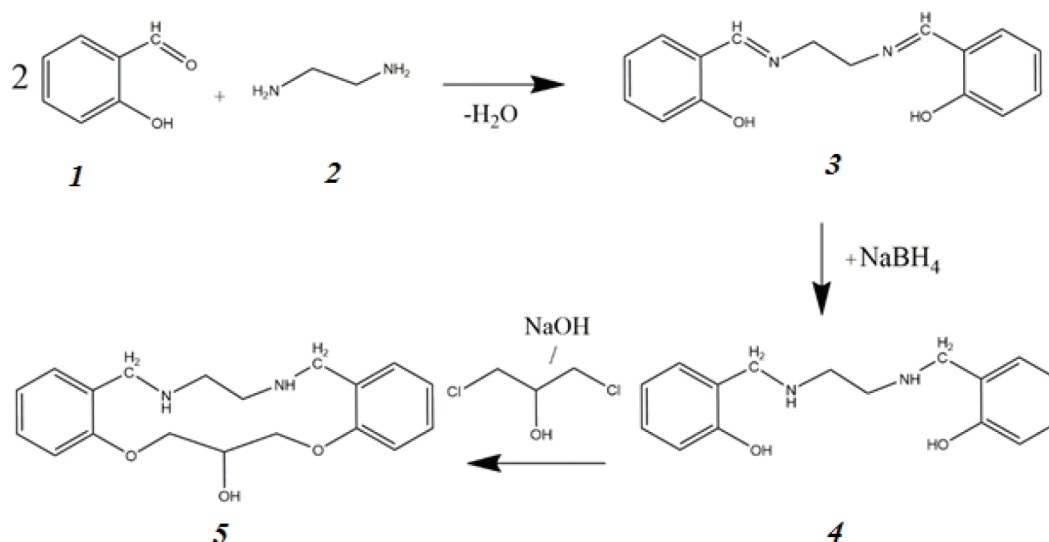
Scheme. The synthesis of 7,8,14,15,16,17,18,19-octahydro-6H-dibenzo[f,n] [1,5,9,12] dioxadiazacyclopentadecin-7-ol (diazacrown ether or DC).

The purity and crystalline properties of the Ag^0 nanoparticles were determined by powder XRD. The XRD patterns are shown in Figure 1. All the XRD peaks were well defined and corresponded to Ag^0 nanoparticles with face-centered cubic structures. The peak broadening in the XRD pattern shows the formation of nanocrystals. In the pattern all lines relate to silver nanoparticles. The pattern has characteristic peaks at 38.3330 (111), 44.480 (200), 64.610 (220), and 77.310 (311) (Table 1) and that correlates well with the standard pattern of silver nanoparticles. The intensity of the diffraction peak of the (111) plane is stronger than the other peaks. The average crystallite size, estimated from the (111) peak using the Williamson–Hall method, is 18.94 Å.
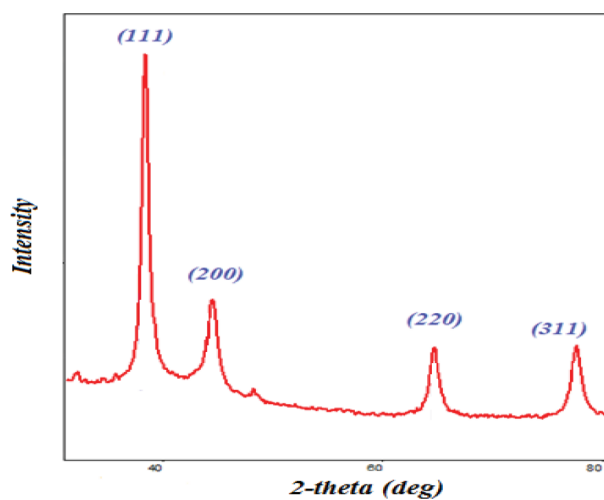

Figure 1. XRD pattern for the nanostructured Ag^0 NPs.

Figure 2 presents the FTIR spectra of DC (a), Ag@DC (b), and Ag^0 nanoparticles (c). The spectrum of starch-reduced Ag^0 nanoparticles (c) reveals the characteristic peak at about 3338–3500 cm^{-1} (–OH stretching).

Table 1. XRD Peak list for Ag^0 NPs.

No.	2-theta (deg)	d (ang)	Height (cps)	FWHM (deg)	Int. I (cps deg)	Int. W (deg)	Asym. factor
1	38.333(17)	2.3462(10)	11687(140)	0.71(2)	13606(134)	1.16(3)	0.97(10)
2	44.48(4)	2.0351(18)	3139(72)	1.18(5)	6045(123)	1.93(8)	1.3(2)
3	64.61(10)	1.4413(19)	1620(52)	1.05(8)	1820(170)	1.12(14)	1.0(4)
4	77.31(4)	1.2332(5)	2284(62)	1.27(15)	5086(263)	2.23(18)	0.32(12)

The spectrum of prepared nanostructures was compared with the spectrum of DC in order to determine the coordination sites of DC that may be involved in chelation with the surface of silver nanoparticles. In the spectrum of the prepared nanostructures the weakening of the intensity of a strong band at 1640 cm^{-1} is seen, corresponding to the secondary NH groups in the DC molecule, and shifts to 1655 cm^{-1}. At the same time, the attenuation of an intensive wide band at 3100–3600 cm^{-1} and the shifting of a band at 1107 cm^{-1}, corresponding to the –OH group of secondary alcohol in the DC molecule, to 1121 cm^{-1} in the spectrum, corresponding to nanostructures, are strong evidence of the coordination of DC molecules with silver nanoparticles via OH and NH groups of DC. The band at 1247 cm^{-1} of the cyclic ether group of DC to 1240 cm^{-1} in the spectra of Ag@DC also confirms the chelation between Ag^0 nanoparticles and DC via noncovalent interaction.
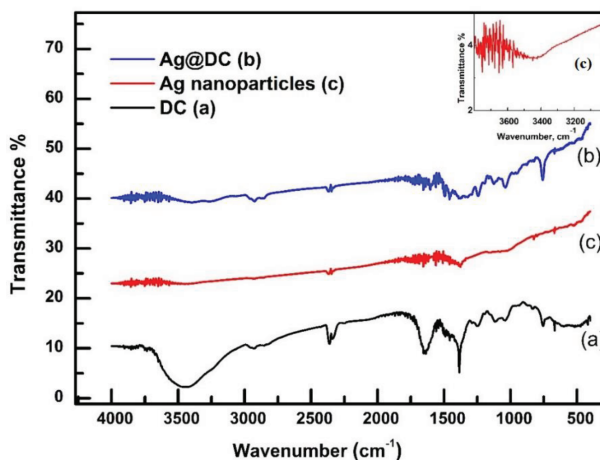
Figure 2. FTIR spectra of a) DC, b) Ag@DC, c) Ag^0 NPs.

UV-spectra of DC and Ag@DC are presented in Figure 3. As can be seen, the characteristic peak of DC is shifted from 275 nm to 260 nm and that may be evidence of the silver nanoparticles' complexation with diazacrown ether.

In Figure 4 the TEM image and size distribution graph of the prepared Ag^0 NPs are presented. As seen from Figure 4, the nanoparticles are homogeneous and the size of the nanostructures varies in the range of 10–18 nm.

The TEM image and size distribution graph of the prepared Ag@DC nanostructures are presented in Figure 5. The nanostructures are also homogeneous and their size varies in the range of 8–18 nm.

The antibacterial activity of the synthesized active agents was studied against *Acinetobacter baumannii* BDU32, *Escherichia coli* BDU12, *Klebsiella pneumoniae* BDU44, *Pseudomonas aeruginosa* BDU49, and
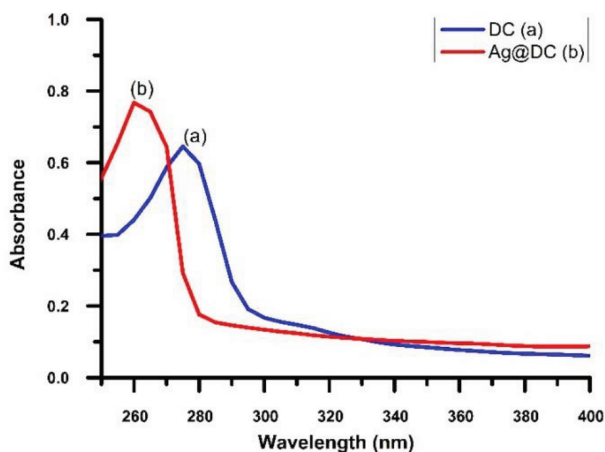
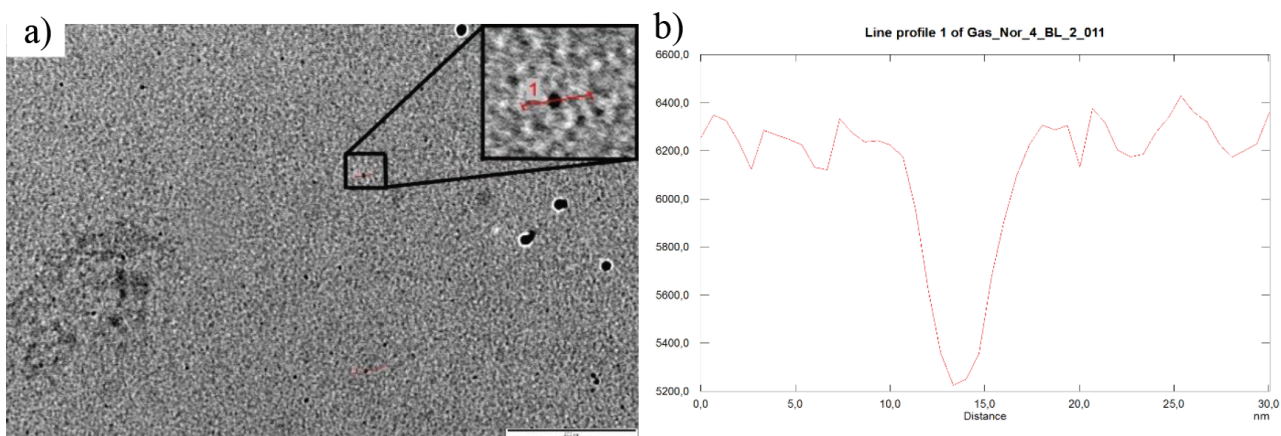**Figure 3**. UV-spectra of a) DC, b) Ag@DC.

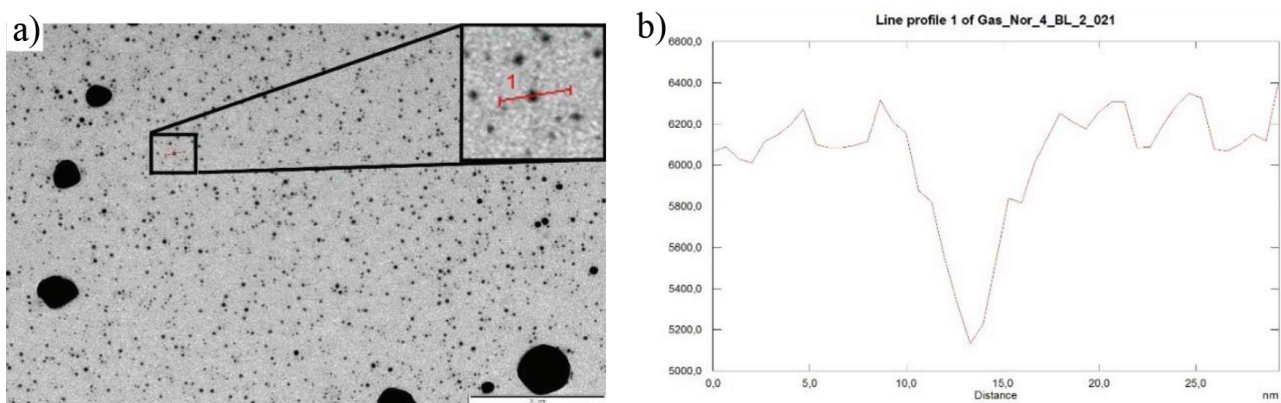**Figure 4**. a) TEM image of Ag^0 NPs; b) size distribution graph of Ag^0 NPs.

Figure 5. a) TEM image of Ag@DC; b) size distribution graph of Ag@DC.

Staphylococcus aureus BDU23 by 96-well microtiter assay. As shown in Table 2, the nanosupramolecular ensemble Ag@DC demonstrated greater antibacterial activity as compared with pure diazacrown-ether (DC) and Ag^0 nanoparticles. Ag@DC showed high activity at the concentration of 2 μg mL^{-1}. In this case, we need to decrease the concentration from 8 to 0.0625 μg mL^{-1} for determining the MIC of this agent. The MIC of Ag@DC against both *E. coli* BDU12 and *S. aureus* BDU23 was 0.125 μg mL^{-1}, whereas the antibacterial effect

was significantly weaker in the case of Ag^0 nanoparticles (4; 64 μg mL^{-1}) and DC (64; 128 μg mL^{-1}). *E. coli* BDU12 and *S. aureus* BDU23 were more susceptible to Ag@DC than other strains. Ag@DC showed equal effect on *A. baumannii* BDU32, *K. pneumoniae* BDU44, and *P. aeruginosa* BDU49 (2 μg mL^{-1}). However, the MIC of Ag nanoparticles for *A. baumannii* BDU32 was 16 times higher and equal to 32 μg mL^{-1}. In the case of *K. pneumoniae* BDU44 and *P. aeruginosa* BDU49, the difference between the MICs of zero-valent silver nanoparticles and Ag@DC was not so impressive, because the MIC of the Ag^0 nanoparticles for both strains was equal to 8 μg mL^{-1}. *E. coli*, *K. pneumoniae*, and *P. aeruginosa* showed higher sensitivity toward Ag^0 nanoparticles in comparison with *A. baumannii* BDU32 and *S. aureus* BDU23. The inhibition activity of DC on *K. pneumoniae* BDU44 and *P. aeruginosa* BDU49 was 128 μg mL^{-1} and against *A. baumannii* BDU44 was 64 μg mL^{-1}. High sensitivity among the bacterial strains was not observed toward DC.

Table 2. Minimum inhibitory concentration (MIC) of tested compounds (μg mL^{-1}).

Bacterial strains	Ag@DC	Ag	DC
Acinetobacter baumannii BDU32	2	32	64
Escherichia coli BDU12	0.125	4	64
Klebsiella pneumoniae BDU44	2	8	128
Pseudomonas aeruginosa BDU49	2	8	128
Staphylococcus aureus BDU23	0.125	64	128

In order to determine the passage and distribution mechanism of Ag@DC, TEM of *Escherichia coli* BDU12 was performed without and after treatment with active agents. The control untreated cells of *E. coli* BDU12 are shown in Figure 6. In Figure 7 slight ultrastructural changes are shown, caused by nanostructures. Ag@DC was located mostly inside the cells. In Figure 8 it is shown that the ultrastructure of bacterial cells was strongly affected by the nanosupramolecular ensemble. As can be seen from this image, the disruption of the cells starts from inside the bacteria, where the nanostructures are mainly concentrated. There is no observed fragmentation of the cell wall of *E. coli* BDU12. In Figure 9 a ghost-cell of *E. coli* BDU12 is demonstrated without inner content. In this case, nanostructures are located in the deformed cell wall.

4. Discussion

According to these results, we can assume that Ag@DC is more effective than Ag^0 and DC against bacterial strains. The results of microbiological studies allow us to assume that the application of diazacrown ether as a chelating agent potentiates the antibacterial effects of silver nanoparticles on gram-positive and gram-negative bacteria. The synergistic effect of Ag@DC nanostructures can be explained by the ionophoric behavior of crown-ethers. Due to their ability to integrate inside the bacterial cell membrane, metal nanoparticles can pass through them inside the cell as if through a sieve.

As a result of the TEM study, it can be assumed that Ag@DC nanostructures perform their action after passing through the cell walls of the bacteria. The enormous difference of 32 times between MICs of Ag^0 nanoparticles and the Ag@DC nanosupramolecular ensemble is explained by the facilitated penetration of silver nanoparticles. A very interesting fact is that nanostructures are abundant inside the cells, indicating that silver nanoparticles in the ensemble are not oxidized to Ag^+ promptly after entering the bacteria. The TEM study of ultrastructural changes of treated *E. coli* BDU12, used as a representative of gram-negative bacteria, also shed
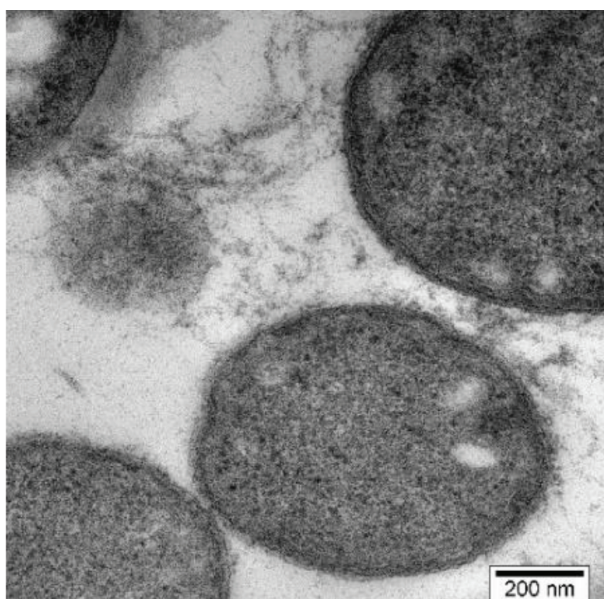
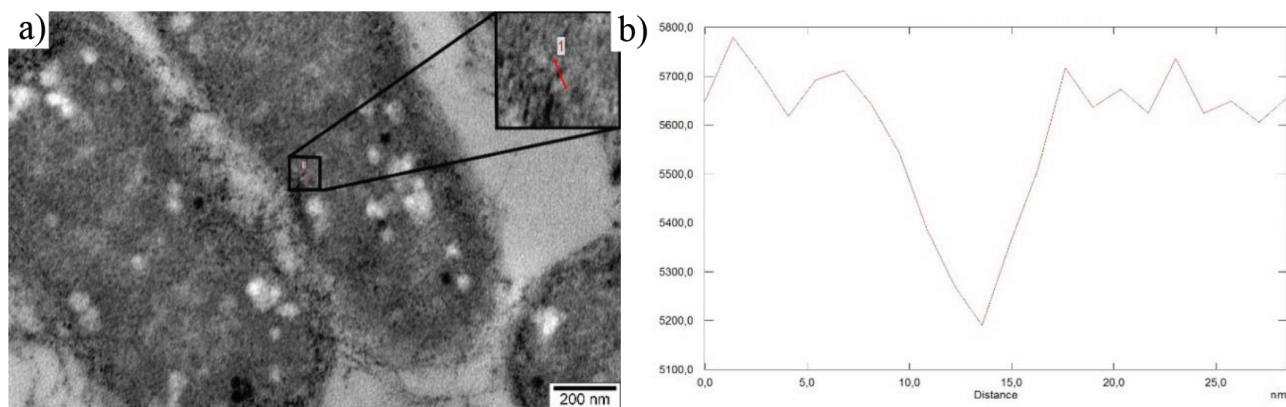**Figure 6**. TEM image of *E. coli* BDU12 without treatment with Ag@DC.

Figure 7. a) Slightly damaged *E. coli* BDU12 cells with Ag@DC nanostructures inside the cells; b) size distribution graph of Ag@DC inside the cell.
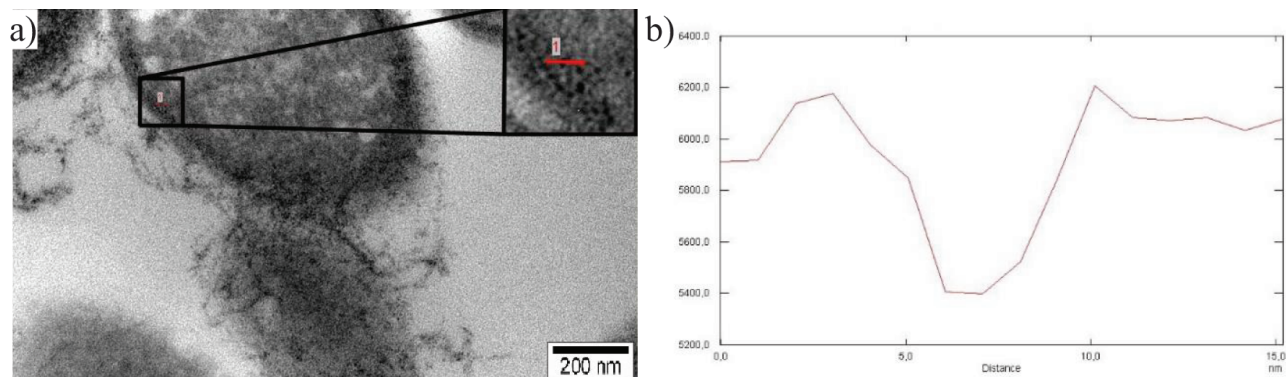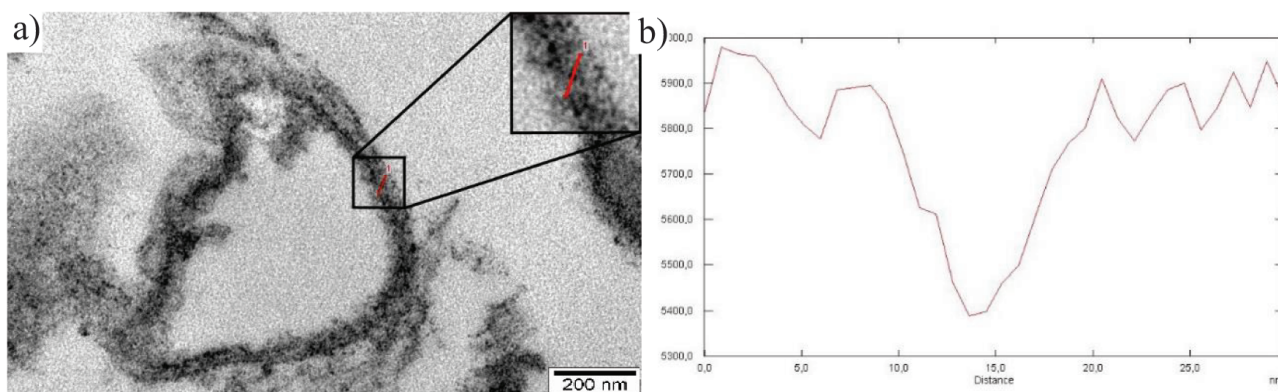

Figure 8. a) Severely damaged *E. coli* BDU12 cells with Ag@DC nanostructures inside the cells; b) size distribution graph of Ag@DC inside the cell.

Figure 9. a) Totally destroyed *E. coli* BDU12 cells with Ag@DC nanostructures inside the cell wall; b) size distribution graph of Ag@DC inside the cell wall.

light on the possible explanation of the higher effectiveness of Ag@DC nanostructures than Ag^0 nanoparticles toward other gram-negative bacteria.

The creation of new active agents on the basis of combining nanotechnology and supramolecular chemical approaches can help to overcome several problems in antimicrobial treatment. Our research shows that it is possible to significantly minimize (from 512 to 4 times in different strains) MICs of silver nanoparticles using the synergistic effect between them and diazacrown ether, which plays the role of a chelating agent. Thus, by chelating silver nanoparticles with a proper agent we can also decrease the therapeutic dose, and in this way reduce their toxicity and adverse effects.

Authors' contributions

S.F. Hajiyeva: Idea, receiving of nanostructures, sample preparation, results analysis, draft and final paper preparation. U.A. Hasanova, Z.O. Gakhramanova: Synthesis of diazacrown ether, draft paper preparation, and approval of the final version. A.A. Israyilova, K.G. Ganbarov: Antibacterial studies, draft paper preparation, and approval of the final version. E.K. Gasimov, F.H. Rzayev: Electron microscopy, draft paper preparation, and approval of the final version. G.M. Eyvazova: IR spectroscopy, draft paper preparation, and approval of the final version. A.E. Huseynzada: Ag^0 nanoparticles synthesis, draft paper preparation, and approval of the final version. G.S. Aliyeva: UV spectroscopy analysis, draft paper preparation, and approval of the final version. I.R. Hasanova: XRD analysis, draft paper preparation, and approval of the final version. A.M. Maharramov: Consulting during research, critical revising of the paper, and approval of the final version.

References

1. Alshehri AH, Jakubowska M, Młozÿniak A, Horaczek M, Rudka D et al. Enhanced electrical conductivity of silver nanoparticles for high frequency electronic applications. ACS Applied Materials & Interfaces 2012; 4 (12): 7007-7010. doi: 10.1021/am3022569

2. Ouyang Z, Li J, Wang J, Li Q, Ni T et al. Fabrication, characterization and sensor application of electrospun polyurethane nanofibers filled with carbon nanotubes and silver nanoparticles. Journal of Materials Chemistry B 2013; 1 (18): 2415-2424. doi: 10.1039/c3tb20316f

3. Gharibshahi L, Saion E, Gharibshahi E, Shaari AH, Matori KA. Structural and optical properties of Ag nanoparticles synthesized by thermal treatment method. Materials 2017; 10 (4): 1-13. doi: 10.3390/ma10040402

4. Warrier P, Teja A. Effect of particle size on the thermal conductivity of nanofluids containing metallic nanoparticles. Nanoscale Research Letters 2011; 6 (1): 247-252. doi: 10.1186/1556-276X-6-247

5. Patil RS, Kokate MR, Jambhale CL, Pawar SM, Han SH et al. One-pot synthesis of PVA-capped silver nanoparticles their characterization and biomedical application. Advances in Natural Sciences: Nanoscience and Nanotechnology 2012; 3 (1): 1-7. doi: 10.1088/2043-6262/3/1/015013

6. Behera S, Nayak PL. Green synthesis and characterization of zero valent silver nanoparticles from the extract of *Vitis vinifera*. World Journal of Nano Science & Technology 2013; 2: 58-61. doi: 10.5829/idosi.wjnst.2013.2.1.211310

7. Mpenyana-Monyatsi L, Mthombeni NH, Onyango MS, Momba MN. Cost-effective filter materials coated with silver nanoparticles for the removal of pathogenic bacteria in groundwater. International Journal of Environmental Research and Public Health 2012; 9 (1): 244-271. doi: 10.3390/ijerph9010244

8. Andrade PF, De Faria AF, Oliveira SR, Arruda MAZ, Do Carmo GM. Improved antibacterial activity of nanofiltration polysulfone membranes modified with silver nanoparticles. Water Research 2015; 81: 333-342. doi: 10.1016/j.watres.2015.05.006

9. Mpenyana-Monyatsi L, Mthombeni NH, Onyango MS, Momba MN. Cost-effective filter materials coated with silver nanoparticles for the removal of pathogenic bacteria in groundwater. International Journal of Environmental Research and Public Health 2012; 9 (1): 244-271. doi: 10.3390/ijerph9010244

10. Ren X, Meng X, Chen D, Tang F, Jiao J. Using silver nanoparticle to enhance current response of biosensor. Biosensors and Bioelectronics 2004; 21 (3): 433-437. doi: 10.1016/j.bios.2004.08.052

11. Sotiriou GA, Pratsinis SE. Engineering nanosilver as an antibacterial, biosensor and bioimaging material. Current Opinion in Chemical Engineering 2011; 1 (1): 3-10. doi: 10.1016/j.coche.2011.07.001

12. Pallaoro A, Hoonejani MR, Braun GB, Meinhart C, Moskovits M. Combined SERS biotags (SBTs) and microfluidic platform for the quantitative ratiometric discrimination between noncancerous and cancerous cells in flow. Biosensing and Nanomedicine V 2012; 8460: 1-8. doi: 10.1117/12.930405

13. Ge L, Li Q, Wang M, Ouyang J, Li X et al. Nanosilver particles in medical applications: synthesis, performance, and toxicity. International Journal of Nanomedicine 2014; 9: 2399-2407. doi: 10.2147/IJN.S55015

14. Chrisnasari R, Wijaya AL, Purwanto MGM. Development of DNA biosensor based on silver nanoparticles UV-Vis absorption spectra for *Escherichia coli* detection. KnE Life Sciences 2015; 2: 382-389. doi: 10.18502/kls.v2i1.180

15. Pallaoro A, Braun G B, Moskovits M. Biotags based on surface-enhanced raman can be as bright as fluorescence tags. Nano Letters 2015; 15 (10): 6745-6750. doi: 10.1021/acs.nanolett.5b02594

16. Li Z, Zhang Y, Ye J, Guo M, Chen J et al. Nonenzymatic glucose biosensors based on silver nanoparticles deposited on TiO_2 nanotubes. Journal of Nanotechnology 2016; 2016: 1-7. doi: 10.1155/2016/9454830

17. Niska K, Knap N, Kędzia A, Jaskiewicz M., Kamysz W et al. Capping agent-dependent toxicity and antimicrobial activity of silver nanoparticles: an in vitro study. Concerns about potential application in dental practice. International Journal of Medical Sciences 2016; 13 (10): 772-782. doi: 10.7150/ijms.16011

18. Xiu ZM, Zhang QB, Puppala HL, Colvin VL, Alvarez PJ. Negligible particle-specific antibacterial activity of silver nanoparticles. Nano Letters 2012; 12 (8): 4271-4275. doi: 10.1021/nl301934w

19. Abramenko N, Demidova TB, Krutyakov YA, Zherebin PM, Krysanov EY et al. The effect of capping agents on the toxicity of silver nanoparticles to *Danio rerio* embryos. Nanotoxicology 2019; 13 (1): 1-3. doi: 10.1080/17435390.2018.1498931

20. Hasanova U, Ramazanov M, Maharramov A, Gakhramanova Z, Hajiyeva S et al. Synthesis of macrocycle (MC) - mimics the properties of natural siderophores and preparation the nanostructures on the basis of MC and magnetite nanoparticles. Chemical Engineering Transactions 2016; 47: 109-114. doi: 10.3303/CET1647019

21. Hasanova UA, Ramazanov MA, Maharramov AM, Gakhramanova Z, Hajiyeva SF et al. The functionalization of magnetite nanoparticles by hydroxyl substituted diazacrown ether, able to mimic natural siderophores, and investigation of their antimicrobial activity. Journal of Inclusion Phenomena and Macrocyclic Chemistry 2016; 86 (1-2): 19-25. doi: 10.1007/s10847-016-0636-x

22. Kumar B, Smita K, Cumbal L, Debut A, Pathak RN. Sonochemical synthesis of silver nanoparticles using starch: a comparison. Bioinorganic Chemistry and Applications 2014; 2014: 1-8. doi: 10.1155/2014/784268

23. Martin A, Takiff H, Vandamme P, Swings J, Palomino JC et al. A new rapid and simple colorimetric method to detect pyrazinamide resistance in *Mycobacterium tuberculosis* using nicotinamide. Journal of Antimicrobial Chemotherapy 2006; 58 (2): 327-331. doi: 10.1093/jac/dkl231

24. Israyilova A, Buroni S, Forneris F, Scoffone VC, Shixaliyev NQ et al. Biochemical characterization of glutamate racemase, a new candidate drug target against *Burkholderia cenocepacia* infections. PLoS One 2016; 11 (11): e0167350. doi: 10.1371/journal.pone.0167350

25. Asadov ZH, Nasibova SM, Rahimov RA, Gasimov EK, Muradova SA et al. Effects of head group on the properties of cationic surfactants containing hydroxyethyl-and hydroxyisopropyl fragments. Journal of Molecular Liquids 2019; 274: 125-132. doi: 10.1016/j.molliq.2018.10.100